Journal of The Electrochemical Society, **151** (6) F135-F140 (2004)
0013-4651/2004/151(6)/F135/6/$7.00 © The Electrochemical Society, Inc.

Interlayer Growth and Electrical Behavior of $Ta_2O_5/SiO_xN_y/Si$ Gate Stacks

Yi-Sheng Lai,[a] J. S. Chen,[a,z] and J. L. Wang[b]

[a]*Department of Materials Science and Engineering, National Cheng Kung University, Tainan, Taiwan*
[b]*Department of Electronic Engineering and Institute of Electronics, National Chiao Tung University, Hsinchu, Taiwan*

Growth and reaction of the interlayer (IL) between ultrathin Ta_2O_5 films and bare, and N_2O or NH_3 plasma-nitrided Si substrate, before and after rapid thermal oxidation (RTO), is examined by X-ray photoelectron spectroscopy. The IL thickness extracted from the attenuated Si 2p photoelectron signal shows that the thermal instability between Ta_2O_5 and Si causes the IL to grow further after RTO annealing. The SiO_xN_y layer formed on the N_2O plasma-nitrided Si appears to provide better barrier efficiency in retarding the growth of IL. For current-voltage measurements, an anomalous saturated current is observed for as-deposited Ta_2O_5 films when stressed positive bias, presumably due to the film/substrate stress-induced Si bandgap widening. After RTO annealing, the leakage current through Ta_2O_5 /IL stacks is higher under positive bias than under negative bias. Ta_2O_5 deposited on N_2O-nitrided Si also exhibits the best leakage behavior among the three systems with the current of 1.7×10^{-8} A/cm^2 at $E = -2.0$ MV/cm and 1.9×10^{-7} A/cm^2 at $E = +2.0$ MV/cm. The correlation between leakage current as well as IL growth is also discussed.
 [DOI: 10.1149/1.1738314]

Manuscript submitted November 3, 2003; revised manuscript received December 12, 2003. Available electronically April 30, 2004.

The steady decrease in geometry scale of microelectronic device places ever-increasing demands on high electrical performance and reliability. In particular, gate oxide thickness is being driven to be less than 20 Å for further ultralarge-scale integrated (ULSI) technology. Within such a scheme, electron tunneling[1] and dopant diffusion[2] through the ultrathin oxide are troublesome. To meet the requirement of low-standby-power devices, high-*k* materials are regarded as gate dielectrics to reduce the tunneling current by increasing its physical thickness. However, recent studies on thermally stable high-*k* materials such as HfO_2, ZrO_2, and metal silicates indicate that an interlayer (IL) is still generated during the deposition and/or subsequent annealing process. To summarize these studies, the degree of IL growth depends mostly on the surface preparation, the deposition, and postannealing conditions.[3-6] The inadvertently grown IL leads to increased equivalent oxide thickness (EOT) and electrical instability during subsequent thermal cycles.

It is realized that successful integration of high-*k* materials into Si devices requires a more detailed understanding of interface engineering.[7] Nitrogen is considered to be the additive to stabilize the gate dielectric either in high-*k* materials or in the IL.[8,9] Many studies reported that nitrogen piled up at the interface retards the growth of SiO_2.[10] Moreover, it also enhances resistance to boron diffusion,[11] increases time-dependent dielectric breakdown,[12] decreases interface state density generation (ΔD_{it}) under electrical stress,[13] and suppresses hot-carrier injection into the oxide.[14] Therefore, interposing a nitrided IL between high-*k* materials and Si substrates gains interest as an alternative application. However, as the nitrogen content increases, it increases the D_{it} of as-grown films and worsens the reliability of negative-bias temperature instability.[15,16]

To have an improved dielectric and leakage characteristics of high-*k* materials, the postannealing process is imperative for repairing the defects in the gate dielectrics. Rapid thermal oxidation (RTO) at high temperature is an effective way to achieve impurity effusion. The amounts of C and H impurities from the metallorganic precursor during the dielectric deposition can be reduced. Moreover, RTO annealing also annihilates defects like vacancies in dielectric films without inducing massive interdiffusion between layers. In this work, ultrathin Ta_2O_5 films deposited on bare Si, plasma N_2O-nitrided Si, and plasma NH_3-nitrided Si followed by RTO annealing at various temperatures and durations were conducted. The plasma nitridation on Si produces a SiO_xN_y interlayer. The reason for using Ta_2O_5 as the dielectric is that Ta_2O_5 is thermodynamically unstable in contact with Si. Consequently, the reaction between Ta_2O_5 and Si is evident and the effectiveness of the SiO_xN_y interlayer on the suppression of IL growth can be clearly resolved.

Experimental

The substrates used were p-type mirror-polished Si(100) wafers. The Si surface was cleaned by a modified Radio Corporation of America (RCA) clean and then dipped in 1% HF solution for 20 s to remove the chemical oxide. Followed by a DI water rinse and N_2 dry, the Si wafer was placed on a 6 in. substrate holder. Nitridation was carried out in a cold-wall, single-wafer plasma-enhanced chemical vapor deposition (PECVD) chamber. Keeping the total pressure at 0.4 Torr and temperature at 450°C, capacitively coupled plasma was generated by a radio frequency (rf, 13.56 MHz) power supply connected to the showerhead plate with a power of 50 W and the substrate holder was grounded. The Si substrate was nitrided in N_2O and NH_3 plasma for 25 s and 5 min, respectively, to produce a 7 Å-thick SiO_xN_y layer. The 7 Å-thick SiO_xN_y layer was interpolated from the parabolic curve for the growth of SiO_xN_y, which was examined by X-ray photoelectron spectroscopy (XPS) and high-resolution transmission micrographs in our previous work.[17] An ultrathin Ta_2O_5 film is then deposited on the bare or nitrided Si substrates by reacting penta-ethoxy-tantalum $[Ta(OC_2H_5)_5]$ with oxygen for 2 min, without exposure to the air. The total chamber pressure was controlled at 1 Torr and temperature was also set at 450°C during Ta_2O_5 deposition. After deposition, Ta_2O_5 films were annealed in a Heatpulse 610i rapid thermal process chamber with flowing dry O_2 at 650 and 800°C. The duration of oxidation was 30 and 90 s.

Chemical bonding states of ultrathin Ta_2O_5 /IL/Si structures were examined by using VG ESCALAB-210 XPS equipped with a 12 kV Al/Mg X-ray source. XPS measurements were performed using Al Kα emission at 1486.6 eV. Figure 1 shows the schematic drawing of the Ta_2O_5 /IL/Si structure, and all the related parameters therein are described later. The thickness of the IL is determined by acquiring the attenuated intensity of Si 2p core-level photoelectrons from the IL (Si^{4+}) and from the Si substrate (Si^0). Because the IL sits underneath the Ta_2O_5 film, the Si 2p core-level intensity I^{4+} for the IL can be expressed by integrating the exponential escape probability and multiplying by the attenuation factor, $\exp(-d_{Ta_2O_5}/\lambda_{Ta_2O_5})$, of the overlayer[18]

[z] E-mail: jenschen@mail.ncku.edu.tw

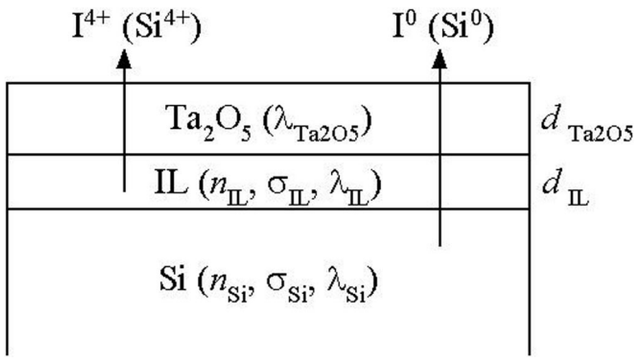

Figure 1. Schematic of the Ta_2O_5 /IL/Si structure comprising a Ta_2O_5 overlayer of thickness, $d_{Ta_2O_5}$, on the top of an IL of thickness, d_{IL}, on the top of the Si substrate. The Si^{4+} photoelectron peak is associated with the Si tetrahedral bonding networks with four foreign atoms from the IL structure and the Si^0 photoelectron peak arises from the pure Si networks of the Si substrate.

$$I^{4+} = n_{IL}\sigma_{IL}\exp(-d_{Ta_2O_5}/\lambda_{Ta_2O_5})\int_0^{d_{IL}}\exp(-z/\lambda_{IL})dz$$
$$= n_{IL}\sigma_{IL}\lambda_{IL}\exp(-d_{Ta_2O_5}/\lambda_{Ta_2O_5})[1-\exp(-d_{IL}/\lambda_{IL})] \quad [1]$$

Likewise, the Si 2p core-level photoemission I^0 from the Si substrate can be written in a similar form except that the escape probability is multiplied by two attenuation factors, namely, $\exp(-d_{Ta_2O_5}/\lambda_{Ta_2O_5})$ and $\exp(-d_{IL}/\lambda_{IL})$, due to the dual Ta_2O_5 /IL overlayers

$$I^0 = n_{Si}\sigma_{Si}\exp(-d_{Ta_2O_5}/\lambda_{Ta_2O_5})\exp(-d_{IL}/\lambda_{IL})\int_0^{\infty}\exp(-z/\lambda_{Si})dz$$
$$= n_{Si}\sigma_{Si}\lambda_{Si}\exp(-d_{Ta_2O_5}/\lambda_{Ta_2O_5})\exp(-d_{IL}/\lambda_{IL}) \quad [2]$$

Dividing Eq. 1 by 2, we obtain

$$\frac{I^{4+}}{I^0} = \frac{I^{4+}_{Si^{4+},\infty}}{I^0_{Si,\infty}}[\exp(d_{IL}/\lambda_{IL})-1] \quad [3]$$

where

$$I^{4+}_{Si^{4+},\infty} = n_{IL}\sigma_{IL}\lambda_{IL} \quad \text{and} \quad I^0_{Si,\infty} = n_{Si}\sigma_{Si}\lambda_{Si}$$

are the photoelectron intensities of an infinitely thick SiO_2 and of a bare Si substrate, respectively. By deriving the equation, we find that the I^{4+}/I^0 ratio is the same whether a Ta_2O_5 overlayer is on top of IL/Si or not, because the intensities I^{4+} and I^0 were all multiplied by a factor, $\exp(-d_{Ta_2O_5}/\lambda_{Ta_2O_5})$. This means that the interlayer between Ta_2O_5 and Si can be fully examined by XPS when the thickness of Ta_2O_5 /IL film stacks is within sixfold inelastic mean-free path length of Si 2p photoelectrons (26 Å for Al Kα radiation). About 99.75% of the total photoelectron signal arises from this sampling depth so that the thickness of the IL could be resolved by Eq. 3. We assume that the IL is mainly composed of SiO_2. The λ_{IL} is then determined to be 26 Å and $(I^{4+}_{Si^{4+},\infty}/I^0_{Si,\infty})$ is 0.82 for Al Kα radiation.[19]

Thicknesses of the Ta_2O_5 /IL stacks were determined using a J. A. Woollam Co., M44 spectroscopic ellipsometer. By applying the refractive index of Ta_2O_5 ($n = 2.25$ at wavelength $\lambda = 527.4$ nm), the dual layers' thicknesses for Ta_2O_5 films deposited on bare Si, plasma N_2O-nitrided Si, and plasma NH_3-nitrided Si are 86, 63, and 68 Å, respectively. To fabricate the metal-oxide-semiconductor (MOS) structure, aluminum dots were deposited on gate stacks. The top electrodes were circular dots of 140 μm diam. The back sides of the wafers were etched in HF solution and then deposited with aluminum to reduce series resistance. The bias was applied to the gate electrode while the substrate in contact with the chuck was connected to the ground. An Agilent 4156B semiconductor parameter analyzer was employed to measure the leakage current for the MOS capacitor. The current-voltage (I-V) measurement was performed with a bias step of 0.1 V, from 0 to −2.5 V, and from 0 to +2.5 V, using a medium integration time.

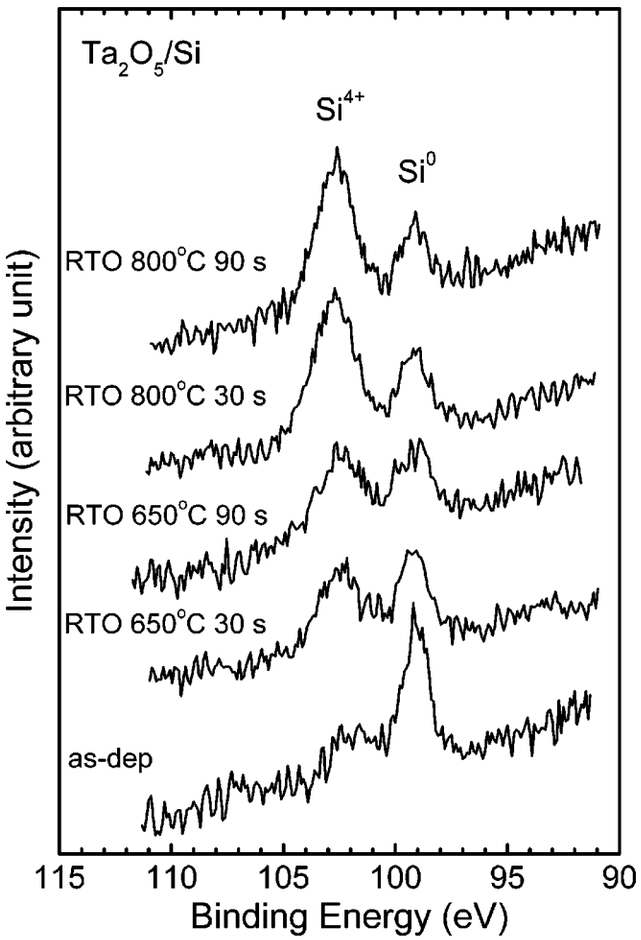

Figure 2. XPS spectra (Al Kα emission at 1486.6 eV) of Si 2p core levels on the surface of ultrathin Ta_2O_5 films deposited on bare Si, before and after RTO annealing at 650/800°C for 30 and 90 s.

Results and Discussion

Effect of RTO temperatures and durations on the IL growth.— Figure 2 shows XPS spectra of Si 2p core levels of ultrathin Ta_2O_5 films deposited on bare Si before and after RTO annealing at 650/800°C for 30 and 90 s. The Si^{4+} peak is associated with the Si tetrahedral bonding networks with four foreign atoms from the IL structure, and the Si^0 peak arises from the pure Si networks of the Si substrate. It is known that the intensity or number of escaped photoelectrons without losing its energy decays exponentially as $(-d/\lambda)$ with its depth d from the surface. The intensity of Si^0 depends on the total thickness of Ta_2O_5 /IL film stacks, whereas that of Si^{4+} depends on the thickness of IL. Because Ta_2O_5 is thermally unstable in contact with Si, an IL forms in as-deposited samples, as seen in Fig. 2. This IL is considered to be a Ta-Si-O layer.[20] Figures

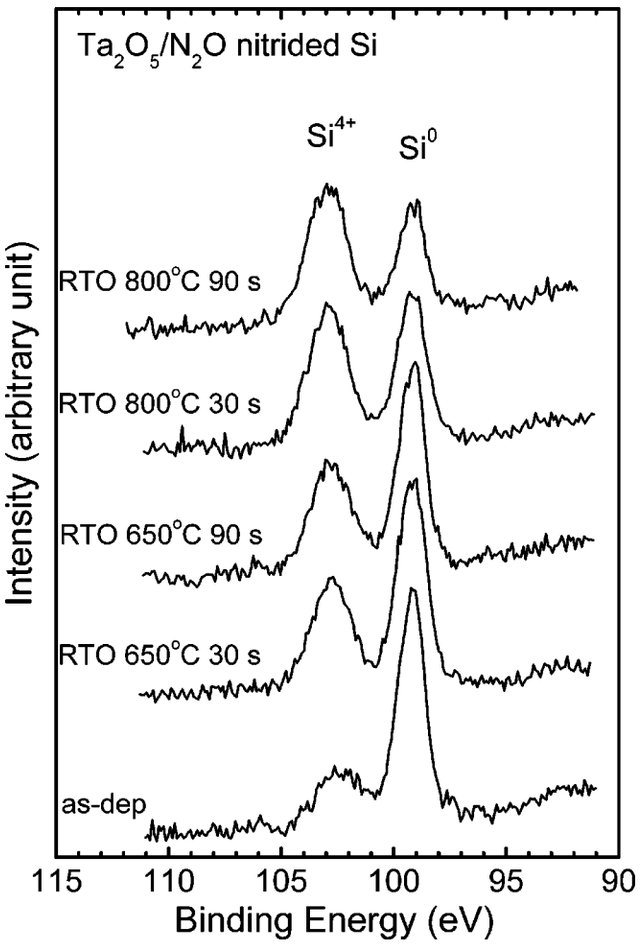

Figure 3. XPS spectra (Al Kα emission at 1486.6 eV) of Si 2p core levels on the surface of ultrathin Ta_2O_5 films deposited on N_2O-nitrided Si, before and after RTO annealing at 650/800°C for 30 and 90 s.

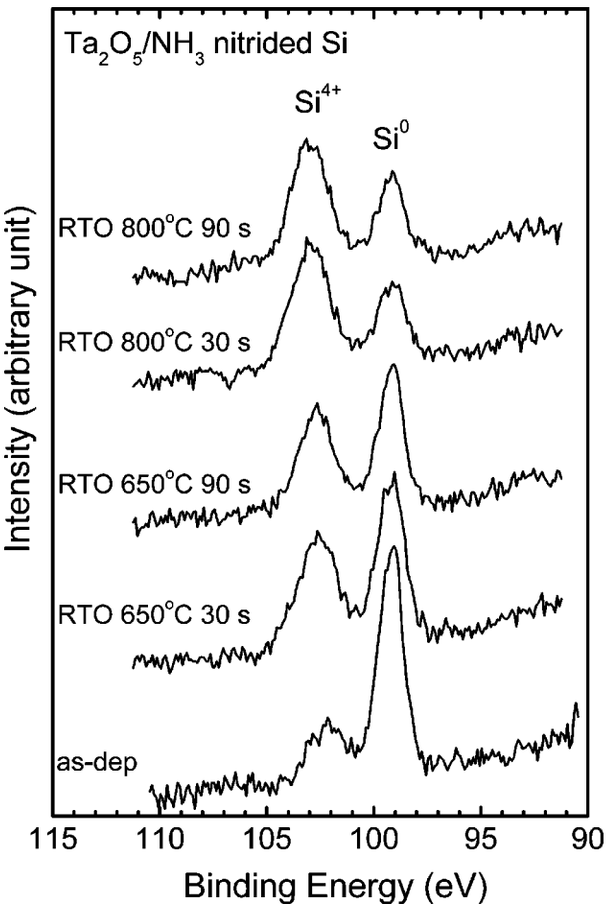

Figure 4. XPS spectra (Al Kα emission at 1486.6 eV) of Si 2p core levels on the surface of ultrathin Ta_2O_5 films deposited on NH_3-nitrided Si, before and after RTO annealing at 650/800°C for 30 and 90 s.

3 and 4 depict XPS spectra of Si 2p core levels of ultrathin Ta_2O_5 films deposited on N_2O- and NH_3-nitrided Si and followed by the same heat-treatment as that of Ta_2O_5/Si. Before Ta_2O_5 film deposition, a 7 Å-thick SiO_xN_y layer was grown as a barrier between Ta_2O_5 and Si. As shown in our previous work, N_2O plasma nitridation produces an oxygen-rich SiO_xN_y layer on Si while NH_3 plasma nitridation forms a nitrogen-rich SiO_xN_y layer.[17] To compare the character of Ta_2O_5/IL in three systems (bare, N_2O-nitrided, and NH_3-nitrided Si), a list of the Si^{4+}/Si^0 intensity ratio and the calculated IL thickness is summarized in Table I.

Table I lists the intensity ratio of Si^{4+} to Si^0 2p core-level photoelectrons before and after RTO annealing in three systems. One can see that the Si^{4+}/Si^0 intensity ratio increases as annealing temperature and time increase, which implies that the growth of IL is both temperature- and time-dependent. It is also found that the IL growth is more sensitive to annealing temperature as compared with annealing time. The most significant IL growth occurs when Ta_2O_5 films were directly deposited on bare Si. On the contrary, after plasma nitriding the Si substrate, the IL growth is inhibited by the nitrogen species piled up at the SiO_xN_y/Si interface.[17] Green *et al.* proposed that nitrogen retards further oxidation by two mechanisms.[21] One is that the nitrogen at the interface may occupy reaction sites and it will constrain the breaking of Si-Si bonds for further reaction. The other is that the nitrogen in SiO_xN_y may inhibit transport of the oxidizing species to the reactive layer. Therefore, the supply of oxidizing gaseous species is limited by their diffusion through the SiO_xN_y layer toward the growing interface. As seen in Table I, N_2O plasma-nitrided SiO_xN_y layer shows the best performance in retarding the growth of the IL. With regard to the NH_3-nitrided system, another species like hydrogen, which is usually introduced during NH_3 plasma nitridation, may assist in the growth of the IL by OH^- radicals. Hydrogen is known to react with O^{2-} to form OH^-, and OH^- radicals are efficient oxidants. In addition, the OH^- solubility is three decades higher than oxygen in SiO_2.[22] The Si-Si backbone would be attacked by the OH^- radicals, and the oxidation rate, in terms of the IL growth, thus increases.[23,24]

Table II shows binding energies (BEs) of Ta $4f_{7/2}$, Ta $4f_{5/2}$, and O 1s core-level electrons from the surface of ultrathin Ta_2O_5 films deposited on bare, N_2O-nitrided, and NH_3-nitrided Si before and after RTO annealing at 650/800°C for 90 s. It is found that as-deposited films usually have lower BEs than films after annealing. The cause may be attributed to the fact that as-deposited Ta_2O_5 films contained more vacancies and further RTO annealing supplies oxygen atoms to repair their oxygen-deficient structure. When Ta_2O_5 films contain increasingly high electronegative oxygen atoms, BEs of Ta $4f_{7/2}$, Ta $4f_{5/2}$, and O 1s core level electrons shift to high values. For stoichiometric Ta_2O_5, the Ta $4f_{7/2}$ and Ta $4f_{5/2}$ BEs are reported to be 26.7 and 28.6 eV,[25] which is near those of high-temperature-annealed Ta_2O_5 films in our work.

Figure 5 shows the XPS spectra of O 1s core-level electrons from the Ta_2O_5/IL/Si structure in three systems. The O 1s peak is composed of signals from the Ta_2O_5 film and the IL. Hence, to understand the bonding configuration before and after RTO anneal-

Table I. Intensity ratio of Si^{4+} to Si^0 2p core-level photoelectron before and after RTO annealing in three systems. The Si^{4+} signal is from the interlayer whereas the Si^0 signal is from the substrate. Increase of the Si^{4+}/Si^0 ratio implies that the IL grows thicker after RTO annealing.

	Ta_2O_5 /Si		Ta_2O_5 /N_2O nitrided Si		Ta_2O_5 /NH_3 nitrided Si	
Condition	Si^{4+}/Si^0	IL (Å)	Si^{4+}/Si^0	IL (Å)	Si^{4+}/Si^0	IL (Å)
As-deposited	0.56	13.6 ± 1.6	0.40	10.4 ± 1.2	0.38	9.8 ± 1.2
650°C, 30 s	1.37	25.6 ± 2.9	0.74	16.8 ± 2.0	1.02	21.1 ± 2.4
650°C, 90 s	1.64	28.6 ± 3.2	0.83	18.1 ± 2.1	1.11	22.3 ± 2.6
800°C, 30 s	2.77	38.4 ± 4.3	1.29	24.6 ± 2.8	2.10	33.0 ± 3.7
800°C, 90 s	3.52	43.3 ± 4.8	1.82	30.4 ± 3.4	2.12	33.2 ± 3.7

ing, a deconvolution process is conducted to resolve the two peaks. The deconvoluted peaks with their BEs and full width at half maximums (fwhms) are summarized in Table II. It is suggested that the intensity of the O 1s peak from the IL increases and shifts to high BEs after RTO annealing, indicative of the growth of IL as well as the increased oxygen content in the stacks. The intensity of ILs for Ta_2O_5 on bare Si is less significant due to the thicker Ta_2O_5 overlayer than the other two systems. It is noted that fwhm's of O 1s and Ta 4f photoelectron peaks are drastically increased for Ta_2O_5 on plasma NH_3-nitrided Si after RTO annealing at 800°C for 90 s. The cause may be due to the outdiffusion of nitrogen in the nitrogen-rich IL.

In summary, an IL appears for as-deposited Ta_2O_5 films in three systems as observed from the small Si^{4+}/Si^0 intensity ratio. It is found that the Si^{4+}/Si^0 intensity ratio increases after RTO annealing at 650/800°C for 30/90 s, irrespective of Ta_2O_5 films deposited on which type of substrates. An increase in the Si^{4+} signal stands for the increase of the IL thickness after heat-treatments. The regrowth of the IL may arise from the migration of substrate Si atoms through the IL to reduce Ta_2O_5 and/or the diffusing of oxidizing species across the ultrathin Ta_2O_5 layer to react with Si substrate. Moreover, it is also revealed that the Si^0 signal decreases at high-temperature annealing, which is also associated with the thickening of Ta_2O_5 /IL stacks after annealing. Because the Si^{4+}/Si^0 ratio increases less in the Ta_2O_5 on plasma N_2O-nitrided Si, an ultrathin plasma N_2O-nitrided SiO_xN_y layer between Ta_2O_5 and Si can retard the IL growth more effectively during heat-treatments.

Current-voltage characteristics.—Figure 6a-c shows J-E curves of three systems before and after RTO annealing at 650/800°C for 30 and 90 s. The trend of the leakage current *vs.* voltage is very similar in the three systems. It is noted that a saturated current was observed for as-deposited films under positive bias. The phenomenon may be associated with film/substrate stress. Su *et al.*[26] addressed that if there is an external tensile stress on the Si substrate, then the Si bandgap is enlarged. The enlargement of the Si bandgap reduces the intrinsic carrier concentration and leads to a lower leakage current. The anomalous behavior of the saturated current disappears after RTO annealing, possibly due to the change of film stress after annealing. In contrast, the as-deposited films exhibited large leakage currents at negative bias and the leakage currents were reduced after RTO. Our previous work demonstrated that Ta_2O_5 films deposited by CVD are oxygen-deficient (O/Ta = 2.44).[27] In addition, from Table II, we observe that the BEs of Ta 4f and O 1s shift to high energy, indicating that Ta_2O_5 films tend toward a more stoichiometric structure after RTO annealing. The reduction of leakage current after postdeposition annealing is generally attributed to the decrease of oxygen vacancies (*i.e.*, more stoichiometric Ta_2O_5) as well as effusion of carbon and hydrogen species within the Ta_2O_5 film.[28]

The leakage current can achieve a relatively low level after RTO annealing at 800°C for 90 s. In the present work, the Ta_2O_5 film deposited on bare Si is thicker than on nitrided Si due to the more significant attenuation of Si^{4+} and Si^0 signals in Fig. 2 than in Fig. 3 and in Fig. 4. However, it exhibited a higher leakage current whether for as-deposited or for annealed samples. The result implicates that a nitrided IL can help reduce the leakage current. Yang *et al.* used the Wentzel-Kramers-Brillouin approximation to calculate the direct-tunneling current for the nitrided interface and found a reduction of tunneling currents by a factor of 8 ± 2 compared with nonnitrided interface.[29] In addition, we had reported that Ta_2O_5 films directly deposited on Si would form a Ta-Si-O IL that is more defective than those when Ta_2O_5 films were deposited on preni-

Table II. BEs and fwhm's of Ta $4f_{7/2}$, Ta $4f_{5/2}$, and O 1s core-level electrons from the surface of ultrathin Ta_2O_5 films deposited on bare, N_2O-nitrided, and NH_3-nitrided Si, before and after RTO annealing at 650 and 800°C for 90 s. The O 1s photoelectron peak is decovoluted into two components representing the signals from the Ta_2O_5 and the IL, respectively.

System	Condition	Ta $4f_{7/2}$ BE/fwhm (eV)	Ta $4f_{5/2}$ BE/fwhm (eV)	O 1s (Ta_2O_5) BE/fwhm (eV)	O 1s (IL) BE/fwhm (eV)
Ta_2O_5 /Si	As-deposited	26.48/1.45	28.36/1.44	530.96/1.57	532.39/1.61
	650°C, 90 s	26.53/1.46	28.41/1.46	531.03/1.56	532.50/1.57
	800°C, 90 s	26.58/1.40	28.46/1.41	531.05/1.57	532.70/1.74
Ta_2O_5 /N_2O nitrided Si	As-deposited	26.48/1.49	28.37/1.49	530.98/1.56	532.46/1.71
	650°C, 90 s	26.59/1.45	28.47/1.45	531.16/1.56	532.61/1.68
	800°C, 90 s	26.71/1.46	28.60/1.45	531.22/1.56	532.76/1.91
Ta_2O_5 /NH_3 nitrided Si	As-deposited	26.52/1.43	28.41/1.42	530.98/1.56	532.39/1.59
	650°C, 90 s	26.57/1.44	28.46/1.44	531.13/1.56	532.58/1.58
	800°C, 90 s	26.63/1.58	28.50/1.51	531.06/2.10[a]	532.64/2.25

[a] This O 1s photoelectron peak should correspond to a partially nitrogen-containing Ta_2O_5 layer because of its wide fwhm. The BE of the peak is also shifted to a low value, suggesting that elements like nitrogen, whose electronegativity is less than oxygen, surround the Ta atoms. The inference is also evident from the wide fwhm's of Ta $4f_{7/2}$ and Ta $4f_{5/2}$ photoelectron peaks.

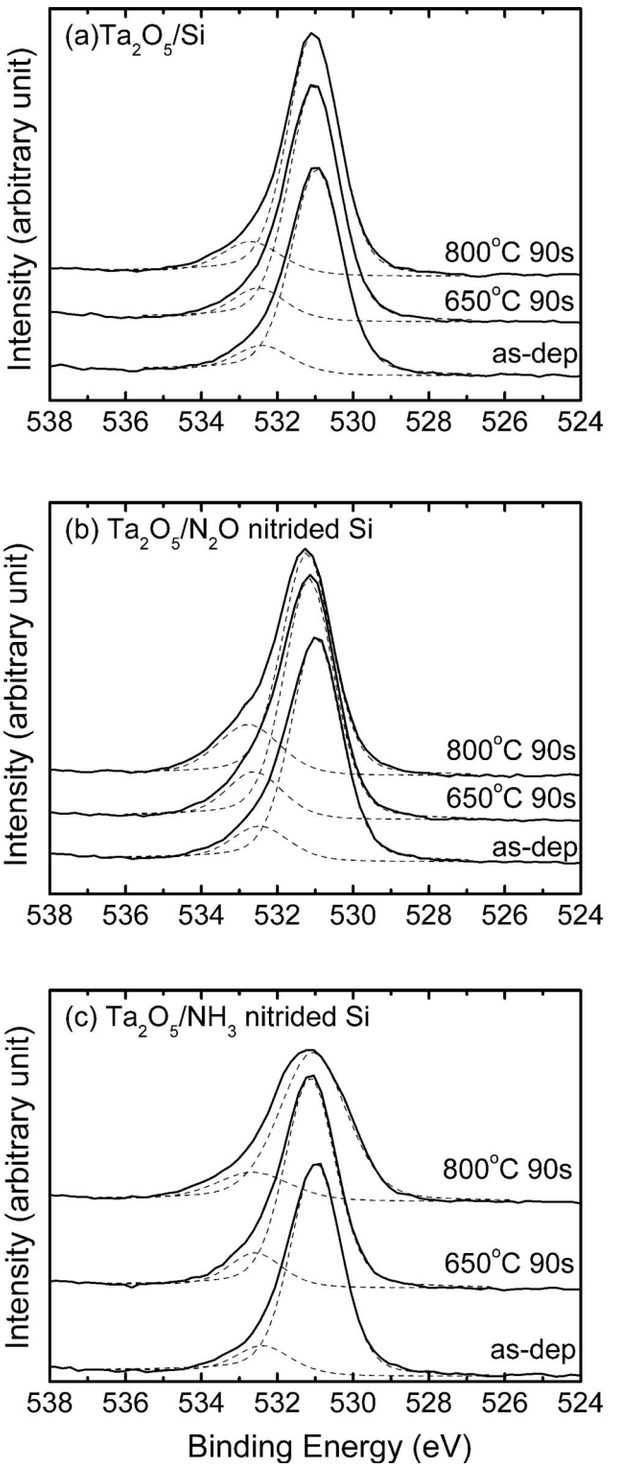

Figure 5. XPS spectra (Al Kα emission at 1486.6 eV) of O 1s core levels on the surface of ultrathin Ta_2O_5 films deposited on (a) bare Si, (b) N_2O-nitrided Si, and (c) NH_3-nitrided Si, before and after RTO annealing at 650 and 800°C for 90 s.

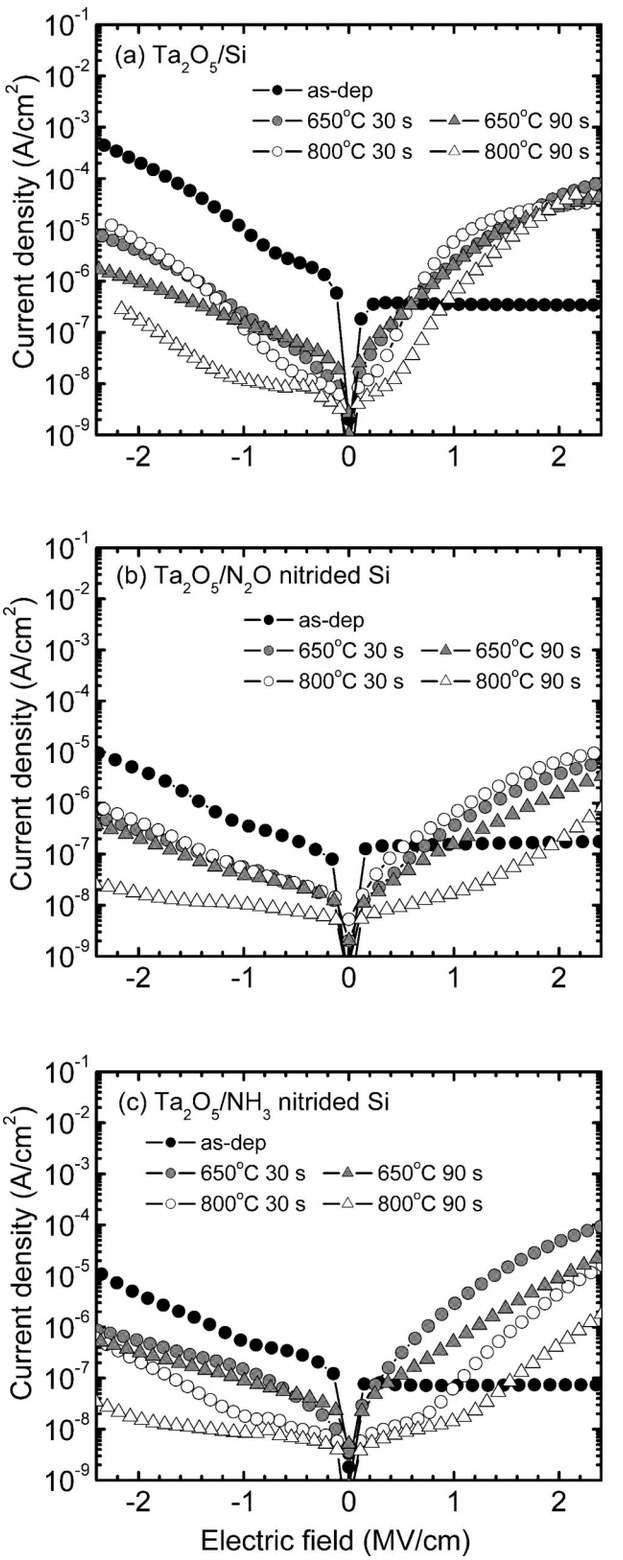

Figure 6. J-E curves of (a) Al/Ta_2O_5/Si, (b) Al/Ta_2O_5/N_2O-nitrided Si, and (c) Al/Ta_2O_5/NH_3-nitrided Si, before and after RTO annealing at 650/800°C for 30 and 90 s. The dielectric thickness is determined by ellipsometry.

trided Si.[30,31] The traps in the defective IL may assist in the electrical carrier transport, and thus increase the leakage current. The two factors may account for the high leakage current in Ta_2O_5 on non-nitrided Si.

Finally, we compare the leakage currents of Ta_2O_5 films deposited on plasma N_2O and NH_3-nitrided Si. From Table I, we realize that the plasma NH_3-nitrided IL grows faster than plasma

N_2O-nitrided IL after annealing. It is proposed that hydrogen may assist in the growth of the IL. It is found from Fig. 6b and c that the leakage current of plasma NH_3-nitrided IL is higher than that of plasma N_2O-nitrided IL when annealing at 650°C. Andrés *et al.* demonstrated that the hydrogen concentration decreases as the rapid thermal annealing temperature increases.[32] At 650°C, considerable hydrogen may outdiffuse from the IL and leave defective sites in the IL. The defective IL could be reorganized by the interface reoxidation after annealing at higher temperature or for longer times. Accordingly, the leakage current of plasma NH_3-nitrided IL is improved as the annealing temperature and duration increase.

Conclusions

In this work, the IL grown beneath Ta_2O_5 films, before and after RTO annealing, is characterized by XPS. The various degrees of IL growth can be attributed to differences in their capability as an efficient barrier against interdiffusion. Results indicate: (*i*) nitrogen at the IL/Si interface is effective to retard the growth of the IL as compared to the non-nitrided system. However, nitrogen in the nitrogen-rich IL may outdiffuse to the Ta_2O_5 overlayer after long-time annealing at elevated temperatures. (*ii*) Hydrogen introduced into the IL via plasma NH_3 nitridation may assist in the growth of the IL, though the IL is nitrogen-rich.

With regard to the J-E performance, a similar trend is found in three systems. However, the SiO_xN_y IL exhibits lower leakage currents than unintentionally grown IL. The reduced direct tunneling current and the less defective structure of nitrided ILs may explain the phenomena. In conclusion, the plasma N_2O-nitrided SiO_xN_y layer preserves a more stable structure with suppression of IL growth as well as lower leakage currents through the gate stacks.

Acknowledgment

The authors gratefully appreciate the financial support from the National Science Council of Taiwan, R.O.C. (grant no. NSC-92-2216-E-006-022).

National Cheng Kung University assisted in meeting the publication costs of this article.

List of Symbols

I^{4+}	integrated photoelectron intensity of the Si^{4+} peak from the IL
I^0	integrated photoelectron intensity of the Si^0 peak from the Si substrate
n_{IL}	density of Si atoms in the IL
n_{Si}	density of Si atoms in the Si substrate
σ_{IL}	Si atomic photoionization cross section in the IL
σ_{Si}	Si atomic photoionization cross section in the Si substrate
λ_{Si}	inelastic mean-free path of photoelectron in the Si
λ_{IL}	inelastic mean-free path of photoelectron in the IL
$\lambda_{Ta_2O_5}$	inelastic mean-free path of photoelectron in the Ta_2O_5
d_{IL}	thickness of the IL
$d_{Ta_2O_5}$	thickness of the Ta_2O_5

References

1. Y.-C. Yeo, T.-J. King, and C. Hu, *IEEE. Trans. Electron Devices*, **50**, 1027 (2003).
2. C. P. Liu, Y. Ma, H. Luftman, and S. J. Hillenius, *IEEE Electron Device Lett.*, **18**, 212 (1997).
3. M. Kundu, N. Miyata, and M. Ichikawa, *J. Appl. Phys.*, **93**, 1498 (2003).
4. Y.-S. Lin, R. Puthenkovilakam, J. P. Chang, C. Bouldin, I. Levin, N. V. Nguyen, J. Ehrstein, Y. Sun, P. Pianetta, T. Conard, W. Vandervorst, V. Venturo, and S. Selbrede, *J. Appl. Phys.*, **93**, 5945 (2003).
5. B.-Y. Tsui and H.-W. Chang, *J. Appl. Phys.*, **93**, 10119 (2003).
6. K.-J. Choi, J.-B. Park, and S.-G. Yoon, *J. Electrochem. Soc.*, **150**, F75 (2003).
7. R. M. C. de Almeida and I. J. R. Baumvol, *Surf. Sci. Rep.*, **49**, 1 (2003).
8. C. S. Kang, H.-J. Cho, K. Onishi, R. Nieh, R. Choi, S. Gopalan, S. Krishnan, J. H. Han, and J. C. Lee, *Appl. Phys. Lett.*, **81**, 2593 (2002).
9. P. D. Kirsch, C. S. Kang, J. Lozano, J. C. Lee, and J. G. Ekerdt, *J. Appl. Phys.*, **91**, 4353 (2002).
10. M. L. Green, E. P. Gusev, R. Degraeve, and E. L. Garfunkel, *J. Appl. Phys.*, **90**, 2057 (2001).
11. C. T. Liu, Y. Ma, H. Luftman, and S. J. Hillenius, *IEEE Electron Device Lett.*, **18**, 212 (1997).
12. M. Beichele, A. J. Bauer, M. Herden, and H. Ryssel, *Solid-State Electron.*, **45**, 1383 (2001).
13. M. Bhat, J. Kim, J. Yan, G. W. Yoon, L. K. Han, and D. L. Kwong, *IEEE Electron Device Lett.*, **15**, 421 (1994).
14. H. Huang, W. Ting, D.-L. Kwong, and J. Lee, *IEEE Electron Device Lett.*, **12**, 495 (1991).
15. D. K. Schroder and J. A. Babcock, *J. Appl. Phys.*, **94**, 1 (2003).
16. S. Fujieda, Y. Miura, M. Saitoh, E. Hasegawa, S. Koyama, and K. Ando, *Appl. Phys. Lett.*, **82**, 3677 (2003).
17. Y.-S. Lai and J. S. Chen, *J. Vac. Sci. Technol. A*, **21**, 772 (2003).
18. J. Himpsel, F. R. McFeely, A. Taleb-Ibrahimi, J. A. Yarmoff, and G. Hollinger, *Phys. Rev. B*, **38**, 6084 (1988).
19. M. F. Hochella, Jr., and A. H. Carim, *Surf. Sci.*, **197**, L260 (1988).
20. G. B. Alers, D. J. Werder, Y. Chabal, H. C. Lu, E. P. Gusev, E. Garfunkel, T. Gustafsson, and R. S. Urdahl, *Appl. Phys. Lett.*, **73**, 1517 (1998).
21. M. L. Green, D. Brasen, L. C. Feldman, W. Lennard, and H.-T. Tang, *Appl. Phys. Lett.*, **67**, 1600 (1995).
22. B. E. Deal and A. S. Grove, *J. Appl. Phys.*, **36**, 3770 (1965).
23. J. Dabrowski, *Silicon Surface and Formation of Interfaces*, J. Dabrowski and H.-J. Müssig, Editors, Chap. 5, World Scientific, Singapore (2000).
24. F.-M. Liu, B. Ren, J.-W. Yan, B.-W. Mao, and Z.-Q. Tian, *J. Electrochem. Soc.*, **149**, G95 (2002).
25. J. F. Moulder, W. F. Stickle, P. E. Sobol, and K. D. Bomben, *Handbook of X-Ray Photoelectron Spectroscopy*, J. Chastain and R. C. King, Jr., Editors, Physical Electronics, Inc., (1995).
26. J.-L. Su, C.-C. Hong, and J.-G. Hwu, *J. Appl. Phys.*, **91**, 5423 (2002).
27. Y.-S. Lai and J. S. Chen, *Thin Solid Films*, **420-421**, 117 (2002).
28. M. Houssa, R. Degraeve, P. W. Mertens, M. M. Heyns, J. S. Jeon, A. Halliyal, and B. Ogle, *J. Appl. Phys.*, **86**, 6462 (1999).
29. H. Yang, H. Niimi, J. W. Keister, G. Lucovsky, and J. E. Rowe, *IEEE Electron Device Lett.*, **21**, 76 (2000).
30. Y.-S. Lai, K.-J. Chen, and J. S. Chen, *J. Appl. Phys.*, **91**, 6428 (2002).
31. Y.-S. Lai, K.-J. Chen, and J. S. Chen, *J. Electrochem. Soc.*, **149**, F63 (2002).
32. E. San Andrés, A. del Prado, I. Mártil, G. González-Diaz, D. Bravo, and F. J. López, *J. Appl. Phys.*, **92**, 1906 (2002).